

Impressive optoelectronic and thermoelectric properties of two-dimensional XI_2 ($X=Sn, Si$): a first principle study

Atanu Beral, Jayanta Bera and Satyajit Sahu*

Department of Physics, Indian Institute of Technology Jodhpur, Jodhpur 342037, India

Abstract

Two-dimensional (2D) metal halides have received more attention because of their electronic and optoelectronic properties. Recently, researchers are interested to investigate the thermoelectric properties of metal halide monolayers because of their ultralow lattice conductivity, high Seebeck coefficient and figure of merit. Here, we have investigated thermoelectric and optoelectronic properties of XI_2 ($X=Sn$ and Si) monolayers with the help of density functional theory and Boltzmann transport equation. The structural parameters have been optimized with relaxation of atomic positions. Excellent thermoelectric and optical properties have been obtained for both SnI_2 and SiI_2 monolayers. For SnI_2 an indirect bandgap of 2.06 eV was observed and the absorption peak was found at 4.68 eV. For this the highest ZT value of 0.84 for p-type doping at 600K has been calculated. Similarly, for SiI_2 a comparatively low indirect bandgap of 1.63 eV was observed, and the absorption peak was obtained at 4.86 eV. The calculated ZT product for SiI_2 was 0.87 at 600K. Both the crystals having high absorbance and ZT value suggest that they can be promising candidates for optoelectronic and thermoelectric devices.

Introduction:

The increasing demand of energy per capita and increasing population are causing rapid depletion of fossil fuel resources. Renewable energy sources are the only self-sustainable solutions for the advanced world. So, interest has been growing towards research and development of renewable energy sources. In this context thermoelectric (TE) materials have shown promise in which electric power can be generated by a temperature difference across the material owing to Seebeck effect which suggests that if there is some temperature difference between the two ends of the material then it can give rise to a potential difference. Efficiency of thermoelectric materials depends on Seebeck coefficient (S), electrical conductivity (σ), absolute temperature (T) and total conductivity (k). High S , σ value, and low k values are required to get good thermoelectric behavior. After the discovery of graphene, many new 2D materials came into existence [1]–[3]. These 2D materials have shown very interesting properties as compared to bulk materials, such as tunable electronic and optoelectronic properties of materials [4], that led to the use of the materials in energy storage [5], and photovoltaic devices [6][7]. Therefore, people have also shown interest to study and enhance the TE efficiency of 2D transition metal dichalcogenides (TMDC) [8],[9], silicene [10], germanene [11], phosphorene [12]. Because of weak VanderWaals interlayer interaction individual layers of these materials can be exfoliated easily with scotch tape [13]. They can also be grown using chemical vapor deposition (CVD) [14] and thermal evaporation [15] method.

Halide based materials have also attracted researchers because of their excellent semiconducting properties. Among them, group-IV diiodide 2D monolayers are showing great optoelectronic behavior. The stability and electronic property of group-IV iodide 2D materials have been predicted recently [16]. All the monolayer materials have indirect band gap which can be tuned with increase in number of layers. Lead iodide is a good layered material having excellent photoluminescence [17] and electroluminescence [18] property. Good photo absorption and thermoelectric efficiency have also been observed at 300K to 900K in PbI_2 [19],[20]. Another same group material GeI_2 has also showed excellent thermoelectric and optical properties [21]. These crystals are showing better thermoelectric and optical properties than well-known TMDCs and other 2D materials. For example, WS_2 monolayer shows ZT value of 0.7 and 0.4 for n-type and p-type doping respectively at an optimum carrier concentration of $3.5 \times 10^{20} \text{ cm}^{-3}$ and at very high temperature of 1500K [22]. PtSe_2 monolayer also shows ZT value of 0.65 and 0.25 at 600K [23]. The performance of 2D materials

can also be enhanced by applying strain. The improvement of thermoelectric performance of PtSe₂ monolayer has also been studied [23]. The strain dependent thermoelectric properties of WS₂ has also been studied [24], which shows a better performance at comparatively low temperature of 900K. Large Seebeck value has been seen by antimonene and arsenene but because of large lattice thermal conductivity, ZT value is approaching to 0.8 and 0.7 at 700K respectively [25]. Group-III chalcogenides also have been found to be potential candidates as thermoelectric materials. InSe monolayer having hexagonal structure shows high ZT factor of 0.54 (0.48) at 700K for p-type (n-type) doping [28].

Here, for the first time we have studied optoelectronic and low temperature thermoelectric properties of 2D monolayer XI₂ (X=Sn and Si) with the help of density functional theory and Boltzmann transport equation. Although various types of 2D materials have been studied but the need of low temperature thermoelectric material was always there. XI₂ are group-IV diiodide materials in which people have already investigated thermoelectric properties of PbI₂ but the main problem with PbI₂ is the toxicity present in lead. In this work we have calculated high thermoelectric figure of merit for SnI₂ and SiI₂ at 600K. At room temperature the maximum ZT is 0.66 (0.35), 0.78 (0.51) for p-type (n-type) SnI₂ and SiI₂ respectively. So, the theoretical investigation of thermoelectric and optical properties has great significance to understand the physical/chemical properties that enhances the thermoelectric efficiency of these materials. These can be used as good thermoelectric materials and used to fabricate devices with excellent efficiency. The absorption peaks occur at ultraviolet region for both materials. So, one of the promising devices that can be fabricated from these materials is a photodetector.

Methodology:

The first principle calculations have been carried out using density functional theory (DFT) with Vanderbilt ultrasoft pseudopotential [29] and Perdew-Burke-Ernzerh (PBE) as generalized gradient approximation (GGA)[30] in Quantum Espresso (QE) package[31]. To avoid periodic boundary approximation and interaction between two layers a sufficient vacuum of 20 Å has been kept along Z direction. The calculations have been performed with 15×15×1 k-mesh sampling with ordinary Gaussian spreading. The atoms were relaxed to their equilibrium position until a force convergence threshold of 10⁻³ eV/Å has been achieved and hence helped in optimizing the cell parameters. A 45×45×1 k-mesh was considered for optical calculation and on-self-consistent calculation. All the

calculations were carried out with 45 Ry cut-off energy and convergence threshold energy for self-consistency was kept at less than 10^{-9} Ry. Phonon band structure was calculated with Density Functional Perturbation Theory (DFPT) as implemented in QE with $6 \times 6 \times 1$ q-mesh grid. The optical properties were calculated by using the Time Dependent Density Functional Perturbation Theory (TD-DFPT) with SIESTA package [32]. Imaginary and real parts of dielectric function were optimized from momentum space formulation and Kramers-Kronig transformation [33] respectively. From dielectric function other optical properties like absorption coefficient (α), refractive index (η), extinction coefficient (K) can be obtained from the following equations.

$$\eta = \left[\frac{\{(\varepsilon_1^2 + \varepsilon_2^2)^{1/2} + \varepsilon_1\}}{2} \right]^{1/2} \quad (1)$$

$$K = \left[\frac{\{(\varepsilon_1^2 + \varepsilon_2^2)^{1/2} - \varepsilon_1\}}{2} \right]^{1/2} \quad (2)$$

$$\alpha = \frac{2K\omega}{c} \quad (3)$$

Where, $\varepsilon_1, \varepsilon_2, \omega, C$ are the real and imaginary functions of dielectric, frequency of incident light, speed of light. Thermoelectric parameters were calculated from Boltzmann transport equation and constant scattering time approximation as implemented in BoltzTraP code [34]. The transport properties can be obtained from the following equations

$$\sigma_{l,m} = \frac{1}{\Omega} \int \sigma_{l,m}(\varepsilon) \left[-\frac{\partial f_{\mu}(T, \varepsilon)}{\partial \varepsilon} \right] d\varepsilon \quad (4)$$

$$k_{l,m}(T, \mu) = \frac{1}{e^2 T \Omega} \int \sigma_{l,m}(\varepsilon) (\varepsilon - \mu)^2 \left[-\frac{\partial f_{\mu}(T, \varepsilon)}{\partial \varepsilon} \right] d\varepsilon \quad (5)$$

$$S_{l,m}(T, \mu) = \frac{(\sigma^{-1})_{n,l}}{e T \Omega} \int \sigma_{n,m}(\varepsilon) (\varepsilon - \mu) \left[-\frac{\partial f_{\mu}(T, \varepsilon)}{\partial \varepsilon} \right] d\varepsilon \quad (6)$$

Where, $\sigma_{l,m}, k_{l,m}, S_{l,m}$ e, T, Ω, μ are the electrical conductivity, electronic thermal conductivity, Seebeck coefficient, electron charge, absolute temperature, volume of the unit cell, chemical potential respectively. In terms of group velocity conductivity tensor can be obtained from the following equation.

$$\sigma_{l,m}(i, \mathbf{k}) = e^2 \tau_{i,\mathbf{k}} v_l(i, \mathbf{k}) v_m(i, \mathbf{k}) \quad (7)$$

Where, v_l is the group velocity, given by

$$v_l(i, \mathbf{k}) = \frac{1}{\hbar} \frac{\partial \varepsilon_{i,\mathbf{k}}}{\partial k_l} \quad (8)$$

Where, k_l is the l^{th} component of wave vector \mathbf{k} and $\varepsilon_{i,\mathbf{k}}$ is the energy of the i^{th} band.

Lattice thermal conductivity (k_{ph}) and phonon lifetime of materials were calculated using supercell approach with phono3py package [35] interfaced with QE. Supercell of $2 \times 2 \times 1$ with k-mesh of $6 \times 6 \times 1$ was constructed and self-consistent calculations of supercells with finite displacement of 0.06 \AA have been included to calculate k_{ph} and lifetime.

Results and Discussions:

Structural properties and mechanical stability:

XI_2 (X=Sn and Si) monolayer has a hexagonal honeycomb like structure with space group 164 (P-3m1). The monolayer has three atomic layers with X as the middle layer and the I atoms constitute the upper and lower atomic layers respectively. So, a unit cell is consisting of one X atom and two I atoms. The side and the top views of the unit cell of XI_2 are shown in fig. 1(a) and (b) respectively. Each X atom is surrounded by six I atoms and the I atoms themselves form closed hexagonal structure. The lattice constants were optimized by relaxing the unit cell. For SnI_2 monolayer, the optimized lattice constants $a=b=4.52 \text{ \AA}$ and height 3.73 \AA were in good agreement with previous experimental results[15]. In each unit cell two different angles 89.27° and 89.0° for $\angle I-Sn-I$ and $\angle Sn-I-Sn$ respectively were obtained. Similarly, for SiI_2 the corresponding optimized lattice constants, angles $\angle I-Si-I$, and $\angle Si-I-Si$ after relaxation are $a=b=4.19 \text{ \AA}$, 90.86° , 89.93° respectively. The distances and angles between atoms are shown in table-1.

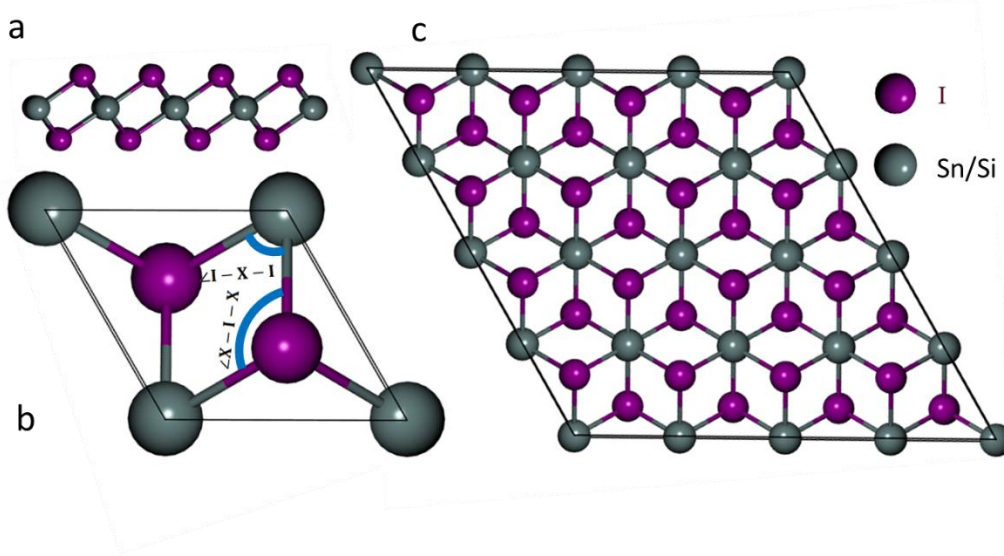


Figure 1. (a) Side view of XI_2 monolayer. (b) The top view of the unit cell which also shows the angles $\angle I-X-I$ and $\angle X-I-X$. (c) The top view of XI_2 super cell, which clearly shows the honeycomb structure.

Crystal	$a=b$ (Å)	d_{X-I} (Å)	d_{I-I} (Å)	Height (Å)	θ_{I-X-I}	θ_{X-I-X}	Cohesive Energy (eV/atom)
SnI ₂	4.52	3.2249	4.5302	3.73	89.27°	89.01°	14.286
SiI ₂	4.19	2.9837	4.1921	3.43	90.84°	89.93°	2.39

Table 1. Structural information of SnI₂, and SiI₂ monolayers.

The cohesive energy calculation of the unit cells gives us the information about the stability of the unit cell which can be obtained by using the following equation: $E_{ch} = \{(E_X + 2.E_I) - E_{XI_2}\}/3$, where E_{XI_2} , E_X , E_I are the total energy of 2D monolayer, isolated X atom, and isolated I atom respectively. Using this we found out the cohesive energy per atom in the 2D monolayer SnI₂ and SiI₂ are 14.286 eV and 2.39 eV respectively, which gives us the information that these structures are stable.

To check the thermodynamical stability due to the vibration of the atoms in the lattice the phonon dispersion data along the high symmetry path Γ -M-K- Γ were studied and is shown for SnI₂ and SiI₂ in fig. 2(a) and (b) respectively. The dynamic stability of the structures were confirmed from the

absence of the imaginary frequencies. Total nine vibrational modes were obtained due to the three atoms in the unit cell, out of which three are acoustic modes and six are optical modes obtained due to the in-phase and out of-phase vibration of the atoms respectively in the unit cell. The three acoustic modes are in plane transverse (TA), and longitudinal (LA) modes, and out of plane mode (ZA). The highest frequency of the optical mode is 150 cm^{-1} for SnI_2 and there is a finite gap between the optical and the acoustic modes. For SiI_2 , the highest frequency for the optical mode is 260 cm^{-1} but in this case the optical and the acoustic modes are overlapping with each other which indicates the scattering of the optical and acoustic vibrations.

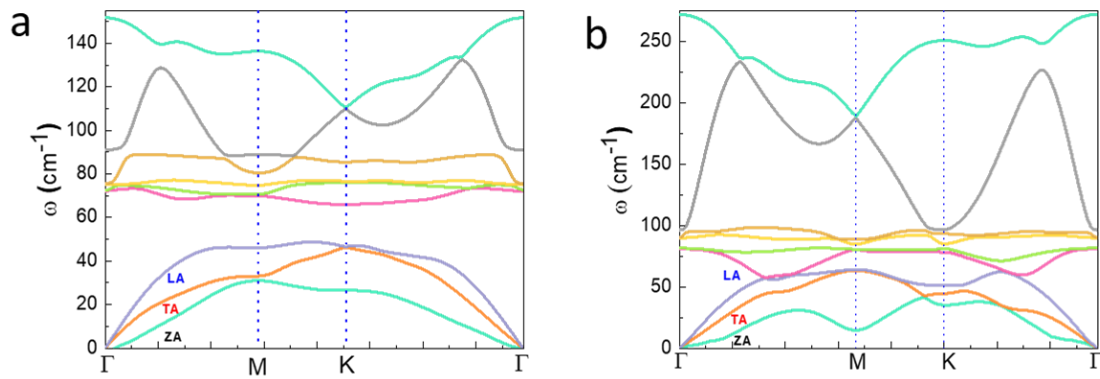


Figure 2. Phonon dispersion curve of (a) SnI_2 monolayer and (b) SiI_2 monolayer. The acoustic in-plane transverse, longitudinal modes and the out of plane mode are shown as TA, LA, and ZA respectively.

Electronic properties:

The electronic band structure of XI_2 monolayer has been studied within the energy range of -5 eV to 5 eV in the first Brillouin zone along the $\text{K}-\Gamma-\text{M}-\text{K}$ path. Fig. 3(a) and (b) show the band structure of SnI_2 and SiI_2 and the corresponding bandgaps are 2.06 eV and 1.63 eV respectively which match well with the previous data [16]. Both the structures show indirect bandgap. For SnI_2 and SiI_2 the valence band maxima (VBM) lies somewhere between the symmetry point K and Γ , whereas the conduction band minima (CBM) lies at Γ point. The valence band has two almost degenerate energy states lying along the $\text{K}-\Gamma$ and $\Gamma-\text{M}$ paths. This is because of the presence of two I atoms.

The projected density of states (PDOS) of SnI_2 in fig. 3(c) indicates that the contribution toward VBM is mainly due to the p_x , p_y and p_z orbitals of I atoms and s orbital of Sn atom. Similarly, the

contribution toward CBM comes mainly from p_x , p_y and p_z orbitals of Sn atom whereas the contribution of p-orbitals of I atoms and s-orbital of Sn atom is negligible. Similarly, for SiI_2 as shown in fig. 3(d) the contribution toward VBM comes mainly from p_x , p_y and p_z orbital of I atom and s orbital of Si atom and the contribution toward CBM comes mainly from p_x , p_z orbitals of Si atom.

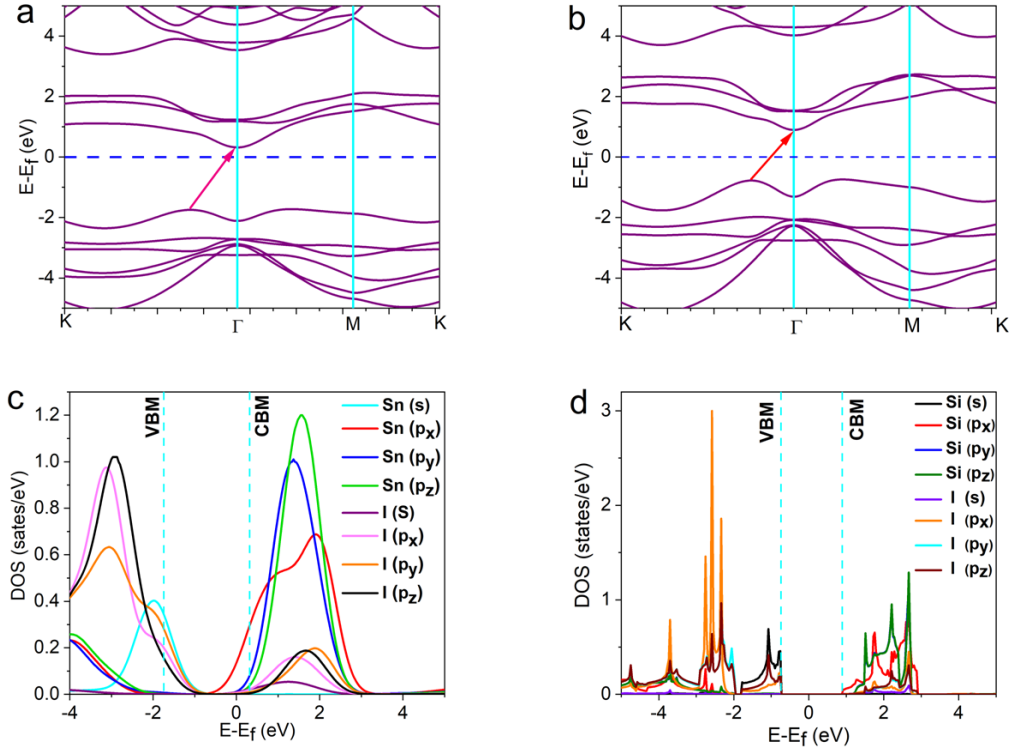


Figure 3. Band structure of (a) SnI_2 monolayer and (b) SiI_2 monolayer. Projected density of state (PDOS) of (c) SnI_2 & (d) SiI_2 monolayer.

Carrier mobility and relaxation time:

Mobility of charge carriers is calculated by using Bardeen and Shockley's deformation potential theory, in which shift in band edge with applied strain can be referred to as deformation potential of the crystal [36]. The expression of mobility for 2D system can be derived from deformation potential and effective mass theorem given as

$$\mu_{2D} = \frac{e\hbar^3 C_{2D}}{K_B T m_e^* m_d (E_f^2)} \quad (9)$$

Here, T is the temperature in Kelvin, $m^* = \frac{d^2E}{dk^2}$ is the effective mass of charge carrier which can be found out from band edge of band structure and average effective mass m_d can be determined as $m_d = \sqrt{m_x^* m_y^*} \cdot \frac{d^2E}{dk^2}$ can be determined by fitting the parabola of band edge of VBM for hole and CBM for electron. $E_I = \frac{\partial V}{\partial \varepsilon}$ is the deformation potential constant of the material, which is calculated from the slope of energy of band edges (V) with applied strain (ε). $C_{2D} = (\partial^2 E / \partial \varepsilon^2) / A_0$ is the elastic constant of 2D monolayer, ε is percentage of strain applied to the system, A_0 is the area of unstrained system. Relaxation time of the charge carrier can be calculated by using the well-known formula $\tau = \frac{\mu m^*}{e}$. All calculated parameters for both the crystals are listed in table 2.

material	$E_{I,electron}$ (eV)	$E_{I,hole}$ (eV)	C_{2D} (J/m ²)	m_e^* (Kg)	m_h^* (Kg)	τ_e (s)	τ_h (s)	μ_e (cm ² V ⁻¹ s ⁻¹)	μ_h (cm ² V ⁻¹ s ⁻¹)
SnI₂	13.684	14.674	87.97	0.271 m ₀	0.337 m ₀	2.08×10 ⁻¹⁴	1.45×10 ⁻¹⁴	135.0	76.05
SiI₂	16.438	17.048	96.06	0.254 m ₀	0.474 m ₀	1.66×10 ⁻¹⁴	0.83×10 ⁻¹⁴	115.75	31.05

Table 2. Calculated deformation potential constant, elastic constant, effective mass, relaxation time, mobility of SnI₂ and SiI₂ monolayer.

Optical properties:

Optical properties of XI₂ (X=Sn and Si) 2D monolayers were calculated along the perpendicular direction of the plane. The imaginary part of dielectric constant(ε_2) is calculated using momentum space formulation with proper matrix elements, whereas real part of dielectric constant(ε_1) has been obtained from Kramers-Kronig transformation. The dielectric function vs energy of incident photon is shown in fig. 4(a). Imaginary part (ε_2) for SiI₂ starts increasing at 1.1 eV and first peak was observed at 3.59 eV with value 4.55, whereas for SnI₂ it started increasing at 1.6 eV and the peak was observed at 3.78 eV with maximum value of 4.37. The energy gap between the two can be explained from the band structure. SnI₂ is having bandgap of 2.06 eV which is 0.43 eV greater than SiI₂ bandgap resulting a blue shift of the bandgap in SnI₂. A secondary peak is observed at 8.09 eV and 8.55 eV for SnI₂ and SiI₂ respectively. The real dielectric constant (ε_1) is finite at zero energy which is 3.13 and 3.85 for SnI₂, and SiI₂ respectively. The peaks are obtained at 2.16 eV and 2.54 eV for SnI₂ and SiI₂ respectively. A negative value for ε_1 can also be seen at 4.59 eV and 5.94 eV which becomes constant after 15 eV.

The absorption spectra are shown in fig. 4(b) which is similar to the imaginary dielectric constant in lower energy region. The first absorption peak was seen at 4.68 eV and 4.86 eV with α value of $5.97 \times 10^5 \text{ cm}^{-1}$ and $6.11 \times 10^5 \text{ cm}^{-1}$ for SnI₂ and SiI₂ respectively, which are of same order as that of GeI₂ [21]. Some secondary peaks are also observed at higher photon energy with lower absorbance and above 25 eV the absorbance is negligible. Hence both the materials can be used in optoelectronic devices. Since the absorption peak is in the UV region hence the materials can be used in UV photodetector. The refractive index with respect to energy is shown in fig. 4(c) which is 1.77 at zero energy and at 2.69 eV it gives the highest value of 2.21 for SiI₂, whereas for SnI₂ the value is 1.96 at zero energy and 2.32 at 2.34 eV. A secondary peak arises at 7.56 eV and 7.33 eV for SiI₂ and SnI₂ respectively. Both the materials have almost constant refractive index of 0.8 after 15 eV.

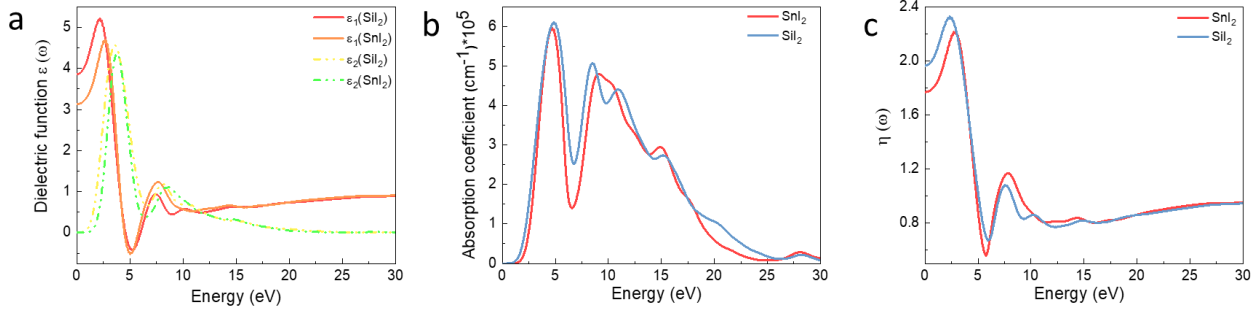


Figure 4. (a) The real part of dielectric function for monolayer SnI₂ (solid red line) and SiI₂ (solid orange line) and imaginary part of dielectric function of SnI₂ (dotted green line) and SiI₂ (dotted yellow line). (b) Absorption coefficient plotted with photon energy of SnI₂ (red line) and SiI₂ (blue line). (c) Refractive index of SnI₂ (red line) and SiI₂ (blue line).

Thermoelectric performance:

One of the important thermoelectric properties to assess the thermoelectric performance of the material is Seebeck coefficient (S). The variation of Seebeck coefficient with chemical potential for SnI₂ is shown in fig. 5(a). The value of S for p-type and n-type carriers in SnI₂ at 300K is 2930 $\mu\text{V/K}$ and 2629 $\mu\text{V/K}$ respectively. With the increase in temperature the value of S decreases because S is inversely proportional to the absolute temperature T. The variation of relaxation time scaled electrical conductivity with chemical potential is shown in fig. 5(b) which hardly changes with the increase in temperature. The electrical conductivity is high for p-type carriers which is 0.91×10^{19} S/m in comparison to n-type charge carriers which is 0.17×10^{19} S/m at the band edges in SnI₂

monolayer. The relaxation time scaled power factor (PF) which is shown in fig. 5(c) is increasing with increase in temperature. The highest value of PF for p-type and n-type carriers at 600K is 21.17×10^{10} W/m-K²-s and 7.63×10^{10} W/m-K²-s respectively. The higher value of $S, \sigma/\tau, S^2\sigma/\tau$ for p-type carriers in comparison to n-type carriers suggest that SnI₂ will be effective as a TE material when doped with p-type material. The S of monolayer SiI₂ at different temperatures are shown in fig. 5(d). The values of S at 300K for p-type and n-type carrier are 2596 μ V/K and 2556 μ V/K respectively and which are higher than that of SnI₂. This can be explained from the perspective of bandgap which is higher for SnI₂ which means there are less number of thermally excited charge carriers near the band edges and Seebeck coefficient is directly proportional to charge. PF for SiI₂ is higher for p-type charge carriers with its maximum value of 23.41 W/m-K²-s. It is observed that the PF is not increasing significantly after 600K for both SnI₂ and SiI₂. So, one can use these materials as low temperature thermoelectric materials. The values of $S, \sigma/\tau, S^2\sigma/\tau$, and ZT product at different temperatures for SnI₂ and SiI₂ are shown in table 3.

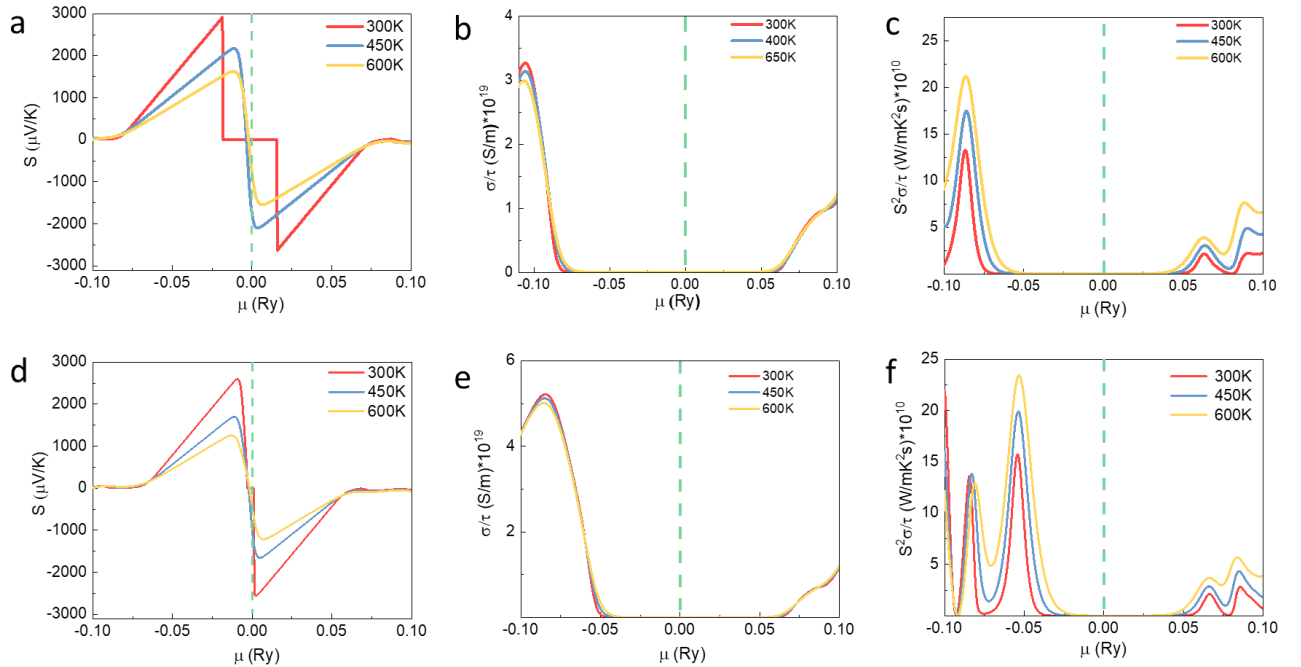


Figure 5. Thermoelectric parameters for SnI₂ are shown in figure (a) to (c) where (a) shows variation of Seebeck coefficient (b) shows variation of σ/τ and (c) variation of $S^2\sigma/\tau$ with chemical potential(μ) at different temperatures. Similarly, for SiI₂ the variation of (d) Seebeck coefficient (e) σ/τ and (f) $S^2\sigma/\tau$ with chemical potential (μ) at different temperatures.

Material		S in ($\mu\text{V/K}$)		$\sigma/\tau * 10^{19}$ (S/m)		$S^2\sigma/\tau * 10^{10}$ (W/mK ² s)		ZT	
		P-type	n-type	P-type	n-type	P-type	n-type	P-type	n-type
SnI ₂	300K	2930	2629	3.26	5.86	13.26	3.89	0.66	0.35
	450 K	2176	2098	3.13	5.75	17.44	4.89	0.78	0.55
	600 K	1623	1545	2.98	5.61	21.17	7.63	0.84	0.65
SiI ₂	300 K	2596	2556	5.21	7.85	15.73	4.07	0.78	0.51
	450 K	1700	1658	5.12	7.72	19.90	6.43	0.84	0.66
	600 K	1255	1215	5.01	7.58	23.41	9.67	0.87	0.74

Table 3. The calculated values of Seebeck coefficient (S), relaxation time scaled electrical conductivity (σ/τ) and power factor ($S^2\sigma/\tau$), thermoelectric figure of merit (ZT) at 300K, 450K, 600K for both p-type and n-type carriers in SnI₂ and SiI₂ monolayers

Lattice thermal conductivity:

Lattice thermal conductivity (k_{ph}) of monolayer XI₂ has been calculated using linear phonon Boltzmann transport equation (LBTE) and relaxation time approximation as implemented in phono3py package. The variation of lattice thermal conductivity with temperature in SnI₂ is shown in fig. 6(a) and the calculated value of k_{ph} is 0.16 W/m-K at 300K. This value is of the same order as that of observed in PbI₂ and GeI₂[21],[37]. The lattice thermal conductivity as a function of temperature in SiI₂ is shown in fig. 6(d) and at 300K the value is 0.05 W/m-K. The variation of thermal conductivity with temperature also follows the same trend as that in SnI₂. The lattice thermal conductivity starts decreasing with increase in temperature. This can be understood from Leibfried and Schlomann's model for lattice thermal conductivity which was modified by Slack [38]. The lattice thermal conductivity for non-metallic crystal is given by

$$k_{ph} = A \frac{\bar{m}\Theta_D^3\delta}{\gamma^2 N^{2/3} T} \quad (10)$$

Where, A is a constant, \bar{m} is average mass per atom in a crystal, Θ_D is Debye temperature, δ is the average volume occupied by one atom, N is number of atoms per unit cell, γ is Gruneisen's constant, the measure of anharmonicity of the crystal[39]. k_{ph} is inversely proportional to temperature which suggests that with increase in temperature the lattice thermal conductivity decreases. The variation of phonon life time and group velocity of SnI₂ with frequency is shown in fig. 6(b) and (c) respectively. The maximum lifetime for phonon is 0.7ps which is much smaller than that of MoS₂, WS₂ and other 2D materials [40], [41]. The maximum phonon group velocity for longitudinal

acoustic modes and optical modes is 2.1 km/s and 4.07 km/s respectively. The phonon life time and the phonon group velocity of SiI_2 are shown in fig. 6(e) and (f). The maximum phonon life time in SiI_2 is 0.3ps, which is smaller than that of SnI_2 . Similarly, the maximum phonon group velocities for the acoustic and optical modes are 3.12 km/s and 12.42 km/s. The lower thermal conductivity can be explained from the point of view of phonon life time, phonon group velocity, and the phonon dispersion relationship as the decrease in the first two causes a decrease in the thermal conductivity. The thermal conductivity of SiI_2 is much smaller than that of SnI_2 and this can be easily related with the comparative life time, and group velocity parameters as for SiI_2 the values for these two are very small. The phonon dispersion curve also suggests that in case of SiI_2 , there is an overlapping between the optical and acoustic modes which causes even more scattering of the phonons and hence lesser transport of the phonons leading to decrease in thermal conductivity.

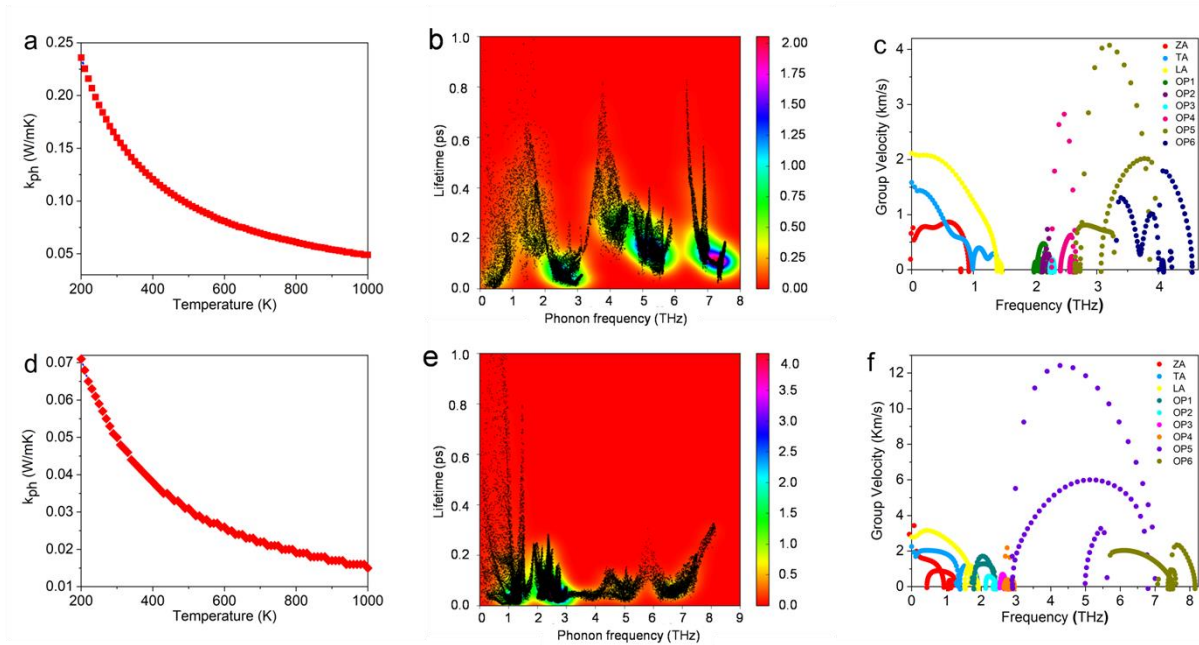


Figure 6. For monolayer SnI_2 (a) The variation of lattice thermal conductivity with temperature. (b) Variation of phonon life time with frequency. (c) Variation of group velocities of various acoustic and optical modes with frequency in monolayer SnI_2 . Similarly, for monolayer SiI_2 (d) The variation of lattice thermal conductivity with temperature. (e) Variation of phonon life time with frequency. (f) Variation of group velocities of various acoustic and optical modes with frequency.

Thermoelectric figure of merit (ZT):

The efficiency of a thermoelectric material called thermoelectric figure of merit (ZT) is calculated by using the parameters we have discussed so far which is related to them as by the following equation:

$$ZT = \frac{S^2 \sigma T}{k} \quad (11)$$

Where S is Seebeck coefficient, σ is the electrical conductivity, T is absolute temperature and k is total thermal conductivity, the sum of both electronic thermal conductivity and lattice thermal conductivity ($k=k_{el}+k_{ph}$). The variation of ZT with chemical potential of SnI₂ and SiI₂ at different temperatures are shown in fig. 7(a) and (b) respectively. Two distinct peaks are observed for each temperature. The peaks in the negative and positive chemical potentials ($\mu < 0$ and $\mu > 0$) are corresponding to the ZT product for p-type and n-type doping respectively. The gap between the two peaks is identical to the energy gap for the corresponding material and in this gap the ZT value is zero. The ZT maxima for the p-type doped SnI₂ are 0.66, 0.78, and 0.84 at 300K, 450K, 600K respectively and for n-type doped SnI₂ it is 0.35, 0.55, and 0.65 at the same corresponding temperatures respectively. These ZT values are much greater than many commonly studied 2D materials [22],[25]. Similarly, for SiI₂ the ZT value maxima for the p-type doped material are 0.78, 0.84, 0.87 and 0.51, 0.66, and 0.74 for n-type doped materials at 300K, 450K, and 600K respectively. As the temperature increases the ZT value also increases but after 600K the value starts to saturate. High ZT product at room temperature suggests that the materials can be used as room temperature thermoelectric material. It is also seen that both the materials have high ZT product when they are doped with p-type materials which suggests that p-type materials behave as better thermoelectric materials. When we look at the thermoelectric properties of both SnI₂ and SiI₂ we see that SiI₂ is a better thermoelectric material than SnI₂.

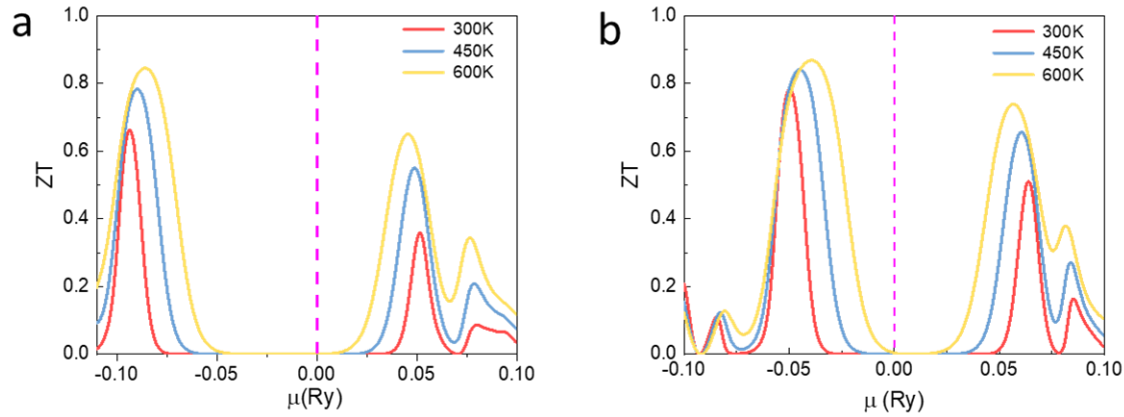


Figure 7. Variation of the thermoelectric figure of merit with chemical potential of material for (a) SnI₂ monolayer (b) SiI₂ monolayer.

Conclusion:

We have calculated the electronic, optical, and thermoelectric properties of SnI₂ and SiI₂ monolayers. Structural parameters were optimized and the dynamical stability was confirmed by studying the cohesive energy and phonon dispersion curve. Both the materials have indirect bandgap with the values of 2.06eV and 1.63eV for SnI₂ and SiI₂ respectively which match with the reported data. The optical properties were calculated and the absorption peak lies in the UV region which prompts that the materials can be used in UV photodetectors. The thermoelectric properties of the materials are impressive having highest power factor of 21.17×10^{10} W/m-K²-s and 23.41×10^{10} W/m-K²-s at 600K for p-type doping for SnI₂ and SiI₂ monolayers respectively. Both the materials show very low lattice thermal conductivity which leads to high ZT product of the value close to the unity, but out of these two materials SiI₂ is a better thermoelectric material because of its lower value of lattice thermal conductivity than that of SnI₂. So, both the materials can be used for high performance thermoelectric device fabrication as well as fabrication of photodetectors in the UV region.

Acknowledgement:

The authors are thankful to Ministry of Human Resource and Development (MHRD) for providing the funding to carry out the research and to Indian Institute of Technology for providing the infrastructure to conduct the research.

References:

- [1] A. K. Geim and K. S. Novoselov, "The rise of graphene," pp. 183–191.
- [2] K. S. Novoselov *et al.*, "Two-dimensional gas of massless Dirac fermions in graphene," vol. 438, no. November, pp. 197–200, 2005, doi: 10.1038/nature04233.
- [3] K. S. Novoselov *et al.*, "Electric field effect in atomically thin carbon films," *Science* (80-.), vol. 306, no. 5696, pp. 666–669, 2004.
- [4] G. A. Tritsarlis, B. D. Malone, and E. Kaxiras, "Optoelectronic properties of single-layer, double-layer, and bulk tin sulfide: A theoretical study," *J. Appl. Phys.*, vol. 113, no. 23, p. 233507, 2013.
- [5] X. Zhang, L. Hou, A. Ciesielski, and P. Samorì, "2D Materials Beyond Graphene for High-Performance Energy Storage Applications," 2016, doi: 10.1002/aenm.201600671.
- [6] S. Roy and P. Bermel, "Electronic and optical properties of ultra-thin 2D tungsten disulfide for photovoltaic applications," *Sol. Energy Mater. Sol. Cells*, vol. 174, pp. 370–379, 2018.
- [7] L. Wang, L. Huang, W. C. Tan, X. Feng, L. Chen, and X. Huang, "2D Photovoltaic Devices : Progress and Prospects," vol. 1700294, pp. 1–20, 2018, doi: 10.1002/smt.201700294.
- [8] W. Huang, X. Luo, C. K. Gan, S. Y. Quek, and G. Liang, "Theoretical study of thermoelectric properties of few-layer MoS₂ and WSe₂," *Phys. Chem. Chem. Phys.*, vol. 16, no. 22, pp. 10866–10874, 2014.
- [9] C. Lee, J. Hong, M. Whangbo, and J. H. Shim, "Enhancing the Thermoelectric Properties of Layered Transition-Metal Dichalcogenides 2H-MQ₂ (M = Mo , W ; Q = S , Se , Te) by Layer Mixing : Density Functional Investigation," vol. 2, 2013.
- [10] K. Zborecki, M. Wierzbicki, and J. Barna, "Thermoelectric effects in silicene nanoribbons," vol. 115404, pp. 1–12, 2013, doi: 10.1103/PhysRevB.88.115404.
- [11] K. Yang, S. Cahangirov, A. Cantarero, A. Rubio, and R. D. Agosta, "Thermoelectric properties of atomically thin silicene and germanene nanostructures," vol. 125403, pp. 1–13, 2014, doi: 10.1103/PhysRevB.89.125403.
- [12] H. Y. Lv, W. J. Lu, D. F. Shao, and Y. P. Sun, "Enhanced thermoelectric performance of phosphorene by strain-induced band convergence," vol. 085433, pp. 1–8, 2014, doi: 10.1103/PhysRevB.90.085433.
- [13] M. Yi and Z. Shen, "A review on mechanical exfoliation for the scalable production of graphene," *J. Mater. Chem. A*, vol. 3, no. 22, pp. 11700–11715, 2015.
- [14] Y. Shi *et al.*, "Synthesis of Few-Layer Hexagonal Boron Nitride Thin Film by Chemical Vapor Deposition," pp. 4134–4139, 2010, doi: 10.1021/nl1023707.

- [15] V. S. Kostko, O. V. Kostko, G. I. Makovetskii, and K. I. Yanushkevich, "Thin film structure of tin(II) iodide," *Phys. Status Solidi Basic Res.*, vol. 229, no. 3, pp. 1349–1352, 2002, doi: 10.1002/1521-3951(200202)229:3<1349::AID-PSSB1349>3.0.CO;2-R.
- [16] M. Naseri, D. M. Hoat, K. Salehi, and S. Amirian, "Theoretical prediction of 2D XI₂ (X=Si, Ge, Sn, Pb) monolayers by density functional theory," *J. Mol. Graph. Model.*, vol. 95, p. 107501, 2020, doi: 10.1016/j.jmgm.2019.107501.
- [17] L. Cabana *et al.*, "Synthesis of PbI₂ single-layered inorganic nanotubes encapsulated within carbon nanotubes," *Adv. Mater.*, vol. 26, no. 13, pp. 2016–2021, 2014.
- [18] B. A. M. Guloy, Z. Tang, P. B. Miranda, and V. I. Srdanov, "A New Luminescent Organic \pm Inorganic Hybrid Compound with Large Optical Nonlinearity **," no. 11, pp. 833–837, 2001.
- [19] B. Peng *et al.*, "High thermoelectric efficiency in monolayer PbI₂ from 300 K to 900 K," *Inorg. Chem. Front.*, vol. 6, no. 4, pp. 920–928, 2019, doi: 10.1039/c8qi01297k.
- [20] D. M. Hoat, T. V Vu, M. M. Obeid, and H. R. Jappor, "Assessing optoelectronic properties of PbI₂ monolayer under uniaxial strain from first principles calculations," *Superlattices Microstruct.*, vol. 130, pp. 354–360, 2019.
- [21] Y.-F. Hu, J. Yang, Y.-Q. Yuan, and J.-W. Wang, "GeI₂ monolayer: a model thermoelectric material from 300 to 600 K," *Philos. Mag.*, vol. 100, no. 6, pp. 782–796, 2020.
- [22] A. N. Gandi and U. Schwingenschlo, "WS₂ As an Excellent High-Temperature Thermoelectric Material," 2014.
- [23] S.-D. Guo, "Biaxial strain tuned thermoelectric properties in monolayer PtSe₂," *J. Mater. Chem. C*, vol. 4, no. 39, pp. 9366–9374, 2016.
- [24] J. Bera and S. Sahu, "Strain induced valley degeneracy: A route to the enhancement of thermoelectric properties of monolayer WS₂," *RSC Adv.*, vol. 9, no. 43, pp. 25216–25224, 2019, doi: 10.1039/c9ra04470a.
- [25] S. Sharma, S. Kumar, and U. Schwingenschlöggl, "Arsenene and antimonene: two-dimensional materials with high thermoelectric figures of merit," *Phys. Rev. Appl.*, vol. 8, no. 4, p. 44013, 2017.
- [26] B. P. Bahuguna, L. K. Saini, R. O. Sharma, and B. Tiwari, "Hybrid functional calculations of electronic and thermoelectric properties of GaS, GaSe, and GaTe monolayers," *Phys. Chem. Chem. Phys.*, vol. 20, no. 45, pp. 28575–28582, 2018.
- [27] M.-S. Li, K.-X. Chen, D.-C. Mo, and S.-S. Lyu, "Predicted high thermoelectric performance in a two-dimensional indium telluride monolayer and its dependence on strain," *Phys. Chem. Chem. Phys.*, vol. 21, no. 44, pp. 24695–24701, 2019.
- [28] N. T. Hung, A. R. T. Nugraha, and R. Saito, "Two-dimensional InSe as a potential thermoelectric material," *Appl. Phys. Lett.*, vol. 111, no. 9, p. 92107, 2017.

- [29] G. Kresse and D. Joubert, "From ultrasoft pseudopotentials to the projector augmented-wave method," vol. 59, no. 3, pp. 11–19, 1999.
- [30] J. P. Perdew, K. Burke, and M. Ernzerhof, "Generalized gradient approximation made simple," *Phys. Rev. Lett.*, vol. 77, no. 18, p. 3865, 1996.
- [31] P. Giannozzi *et al.*, "QUANTUM ESPRESSO: a modular and open-source software project for quantum simulations of materials," *J. Phys. Condens. matter*, vol. 21, no. 39, p. 395502, 2009.
- [32] J. M. Solar *et al.*, "The SIESTA Method for Ab initio," *Order-N Mater. Simulation. J. Phys Condens. Matter*, vol. 14, p. 2745, 2002.
- [33] B. A. Boukamp, "A linear Kronig-Kramers transform test for immittance data validation," *J. Electrochem. Soc.*, vol. 142, no. 6, pp. 1885–1894, 1995.
- [34] G. K. H. Madsen and D. J. Singh, "BoltzTraP. A code for calculating band-structure dependent quantities," *Comput. Phys. Commun.*, vol. 175, no. 1, pp. 67–71, 2006.
- [35] L. Chaput and I. Tanaka, "Distributions of phonon lifetimes in Brillouin zones," vol. 094306, 2015, doi: 10.1103/PhysRevB.91.094306.
- [36] J. Bardeen and W. Shockley, "Deformation potentials and mobilities in non-polar crystals," *Phys. Rev.*, vol. 80, no. 1, p. 72, 1950.
- [37] R. Ran, C. Cheng, Z.-Y. Zeng, X.-R. Chen, and Q.-F. Chen, "Mechanical and thermal transport properties of monolayer PbI₂ via first-principles investigations," *Philos. Mag.*, vol. 99, no. 10, pp. 1277–1296, 2019.
- [38] G. A. Slack, "Nonmetallic crystals with high thermal conductivity," *J. Phys. Chem. Solids*, vol. 34, no. 2, pp. 321–335, 1973.
- [39] N. Mounet and N. Marzari, "First-principles determination of the structural, vibrational and thermodynamic properties of diamond, graphite, and derivatives," pp. 1–14, 2005, doi: 10.1103/PhysRevB.71.205214.
- [40] Y. Cai, J. Lan, G. Zhang, and Y.-W. Zhang, "Lattice vibrational modes and phonon thermal conductivity of monolayer MoS₂," *Phys. Rev. B*, vol. 89, no. 3, p. 35438, 2014.
- [41] X. Gu and R. Yang, "Phonon transport in single-layer transition metal dichalcogenides: A first-principles study," *Appl. Phys. Lett.*, vol. 105, no. 13, p. 131903, 2014.